Micro-Scale Ceramic Additive Manufacturing for Aerospace Applications

CNF Summer Student: Elizabeth Quansah
Student Affiliation: MSE, University of Illinois at Urbana-Champaign

Summer Program(s): 2024 Cornell NanoScale Facility Research Experience for Undergraduates (CNF REU) Program

Principal Investigator(s): Sadaf Sobhani, Department of Mechanical and Aerospace Engineering, Cornell University
Mentor(s): Giancarlo D'Orazio, Department of Mechanical and Aerospace Engineering, Cornell University

Primary Source(s) of Research Funding: National Science Foundation under Grant No. NNCI-2025233

Contact: elizaq99@gmail.com, sobhani@cornell.edu, gd373@cornell.edu

Summer Program Website: https://cnf.cornell.edu/education/reu/2024
Primary CNF Tools Used: Nanoscribe Photonic Professional GT2, Zeiss Ultra Scanning Electron Microscope

Abstract:

This paper suggests mechanisms for producing silica glass microscale electrospray emitters for spacecraft propulsion systems and prefaces the potential of these methods for producing microscale ceramics. The following research is conducted in an effort to replace tungsten needles currently used as emitters and explore micro-scale additive manufacturing. This work relies on two-photon photolithography for additive manufacturing green bodies that undergo thermal processing to produce silica glass, silicon carbide (SiC), or silicon oxycarbide (SiOC). GP Silica, a polymer-based resin containing glass nanoparticles, is converted into emitter-shaped green bodies using the Nanoscribe Photonic Professional GT2. Conversion of SiC and SiOC precursor resins into green bodies using the Nanoscribe is also attempted as in previous works [1-3], and the SiOC precursor exhibits success. Thermally processing green bodies is completed in an air furnace to produce glass and a microwave furnace to produce SiC and SiOC. Characterization of resulting structures suggests high potentials for additively manufacturing glass and thermally processing ceramics in the microwave furnace, although further optimizations remain necessary.

Summary of Research:

Additive manufacturing demonstrates increasing promise for device fabrication, making identifying technological limitations of interest. The Nanoscribe Photonic Professional GT2, a micro-additive manufacturing technology utilizing two-photon photolithography, fires a 780 nm femtosecond laser that is re-emitted at 390 nm after striking a molecule within the resin it is printing with. This provides sufficient energy to cure the resin. This paper explores the Nanoscribe's ability to micro-additively manufacture green bodies for thermal processing to make silica glass, silicon carbide (SiC), and silicon oxycarbide (SiOC).

GP Silica is a polymer-based resin containing glass nanoparticles. Developing emitter green bodies with this resin requires optimizing print parameters using the 10X large feature objective. This was completed by printing a 4 x 4 array of 150 μm cubes on a silicon substrate. Scan speed varied along one axis and laser power along the other. 60% laser power and 80,000 μm/s scan speed produced the smoothest edges and fewest bubbles.

The array was placed in a Nabertherm air furnace for thermal processing according to NanoGuide's standard curve [4], which peaks at 1300°C with 3 hour holds at 90°C, 150°C, 230°C, and 280°C. Following sintering, the array was imaged under the scanning electron microscope (SEM), revealing that 14/16 cubes survived, 12 of which were smooth without cracks or bubbles (Figure 1).

Due to this success, solid glass emitters with a 1000 μm base, 700 μm height, and 20° cone angle were attempted using the same process (Figure 2). Many emitters survived, although deformed, as signified by an estimated 55% shrinkage instead of the expected 30%. Next, a new batch of solid emitters and emitters with porous exteriors were printed and heated for 20 hours in the air furnace according to NanoGuide's fast curve4, which ramps to 1300°C at 180°C/hr, saving approximately 40 hours compared to the standard curve. These emitters were more successful, as demonstrated by an estimated 24% shrinkage (Figure 3).

To determine whether a similar process is possible for producing SiC and SiOC emitters, SiC and SiOC precursor resins were developed for printing on the Nanoscribe with 63X oil immersion on glass substrates. Starfire SMP-10 and Starfire SPR-688 were homogenized into resins by mixing in 1%/wt 2-Isopropylthioxanthone and 9%/wt 1,6-Hexanediol diacrylate. Attempting to print with the SiC precursor Starfire SMP-10 based resin using a 10,000 μm/s scan

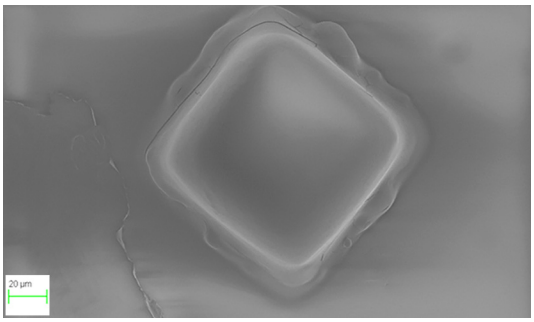

Figure 1: A successful glass cube has a smooth surface without cracks and bubbles.

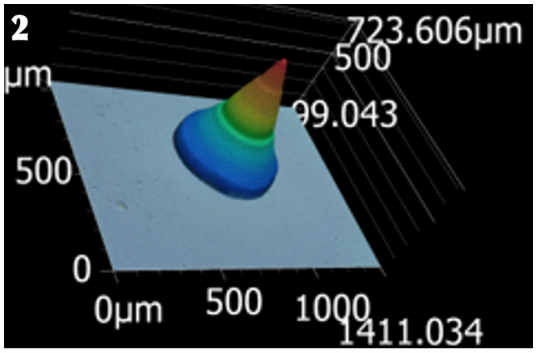

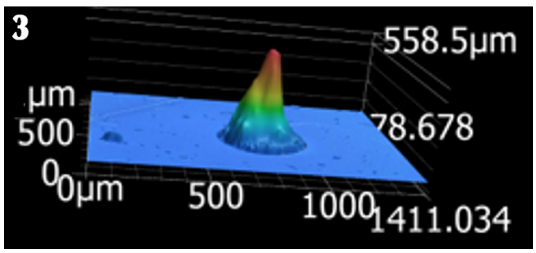

Figure 2: Keyence image of a GP Silica solid emitter green body. Figure 3: Keyence image of a solid glass emitter.

Figure 4: The alumina crucible is lined with SiC and goes inside of a 1 kW microwave.

speed with laser power ranging from 30% to 80%, as well as a 20,000 μm/s scan speed with 70% and 80% laser power produced no parts due to the resin's low viscosity. Significant motion during printing prevented proper curing and substrate adhesion. When printing with the SiOC precursor Starfire SPR-688 based resin, bubbling occurred at laser powers above 50% with a 10,000 μm/s scan speed, suggesting that printing is possible with the SiOC precursor but not the SiC precursor for the formulations and settings tested.

Lastly, the microwave furnace, an alumina crucible lined with SiC within a 1 kW microwave that ramps at 150°C/min, was evaluated for thermal processing ceramics. SiC precursor Starfire SMP-10 cured at 200°C and SiOC precursor Starfire SPR-688 cured at 445°C were placed into the microwave furnace independently for 2, 3, 4, and 5 minutes. Examining 4-minute thermally converted SiC precursor optically and using the SEM revealed consistency with SiC and an amorphous silicate phase. Similarly, 3-minute thermally converted SiOC precursor appeared consistent with SiOC after optical examination.

Conclusions and Future Steps:

In conclusion, GP Silica is useful for micro-additively manufacturing glass emitters with the Nanoscribe. The fast heating curve [4] proves effective as demonstrated by the emitters' 24% shrinkage. Additionally, printing was achieved with the SiOC precursor resin, but not the SiC precursor resin.

Finally, the microwave furnace may present an option for sintering ceramics, but further research is required. In the future, optimizing thermal processing glass emitters and developing emitters using the SiOC precursor resin is necessary, along with testing this process with a more viscous SiC precursor resin.

Acknowledgements:

Many thanks to the CNF REU Program of the National Nanotechnology Coordinated Infrastructure funded by National Science Foundation grant no. NNCI-2025233. Special thanks to Sadaf Sobhani, Giancarlo D'Orazio, Giovanni Sartorello, and Melanie-Claire Mallison for their guidance.

References:

[1] J. Bauer, et al., "Additive manufacturing of ductile, Ultrastrong polymer-derived nanoceramics," Matter, vol. 1, no. 6, pp. 1547–1556, Dec. 2019. doi:10.1016/j.matt.2019.09.009.

[2] G. Konstantinou, et al., "Additive micro-manufacturing of crack-free PDCS by two-photon polymerization of a single, low-shrinkage Preceramic Resin," Additive Manufacturing, vol. 35, p. 101343, Oct. 2020. doi:10.1016/j.addma.2020.101343.

[3] L. Brigo et al, "3D Nanofabrication of SiOC Ceramic Structures," Advanced Science, vol. 5, (12), 2018/12//. Available: https://www.proquest.com/scholarly-journals/3d-nanofabrication-sioc-ceramic-structures/docview/2262718647/se-2.

[4] NanoGuide Professional Photonic Series. (n.d.). Retrieved July 8, 2024, from https://support.nanoscribe.com/hc/en-gb/articles/4402084033810-Printing-with-the-Glass-Printing-Explorer-Set-GP-Silica.

Synthesis of Temperature-Responsive Hydrogel Particles for Hydraulic Control of Cooled Short Circuits

CNF Project Number: 1356-05
Principal Investigator(s): Ulrich Wiesner
User(s): Danni Tang

Affiliation(s): Department of Materials Science and Engineering, Cornell University

Primary Source(s) of Research Funding: U.S. Department of Energy (DOE), Office of Energy Efficiency and Renewable Energy (EERE), Office of Technology Development, Geothermal Technologies Program (DE-EE0009786.000)

Contact: ubw1@cornell.edu, dt427@cornell.edu

Research Group Website: http://wiesner.mse.cornell.edu/

Primary CNF Tools Used: Heidelberg DWL2000, ABM Mask Aligner, AMST MVD100

Abstract:

The "short circuit" issue is one of the major challenges that prevents Enhanced Geothermal Systems (EGS) from being commercially successful. In this work, temperature-responsive poly(N-isopropylacrylamide) (pNIPAM)-based hydrogel particles were designed to mitigate the issue by reducing the local permeability of "short circuit" regions. To understand the particle jamming behavior, we fabricated a parallel step emulsifier device at CNF to produce particles with narrow size distribution to conduct fundamental rheology tests.

Summary of Research:

The "short circuit" issue arising from uneven permeability distributions within fracture systems is one of the major challenges in Enhanced Geothermal Systems (EGS). When a fluid gets injected underground, it preferably flows through highly permeable paths. As a result, these regions are rapidly drained of heat, leading to a premature thermal breakthrough and system failure [1]. To alleviate this problem, we designed temperature-responsive nanocomposite poly(N-isopropylacrylamide) (pNIPAM)-based microgel particles. As one of the most studied thermosensitive hydrogel, pNIPAM exhibits a reversible entropy-driven volume phase transition, leading to particle expansion at low temperatures and particle contraction at high temperatures [2]. With careful design, these pNIPAM-based particles can expand to up to several hundred times their original volume when the temperature of their local environment falls below a threshold. This could effectively diminish short circuits by decreasing local channel permeability.

Particles with varying compositions were successfully synthesized through inverse suspension polymerization (Figure 1a). Single-particle studies conducted under an optical microscope demonstrated the particle's responsiveness to temperature changes (Figure 1b). However, studying the rheological property of jammed particles remained challenging since inverse suspension polymerization yields highly polydisperse particle sizes (Figure 2). With the aim of better understanding this complex hydrogel particle system, it is desirable to also study a simpler case consisting of monodisperse particles. To facilitate particle production with a narrow size distribution, we fabricated a parallel step emulsifier device using CNF tools.

At CNF, the Heidelberg DWL2000 was used to create photomasks based on the CAD design (Figure 3) adapted from Stolovicki, et al. [3]. Next, a two-layer SU-8 master mold was fabricated in the Class II photoresist room following the procedure described in Figure 4. The resulting mold was subsequently treated with (1H,1H,2H,2H-perfluorooctyl) trichlorosilane (FOTS) to increase its hydrophobicity. Lastly, the device was obtained by casting PDMS onto the master mold. In the next step, microgels with different compositions will be produced using this device for rheology tests.

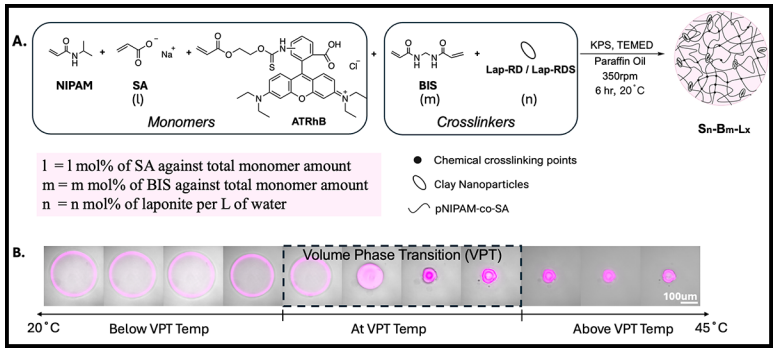

Figure 1: Synthesis of the poly(N-isopropylacrylamide) (pNIPAM)-based nanocomposite microgel. (A) General synthesis scheme of the hydrogel particles. (B) Typical volume phase transition observed under the confocal microscope.

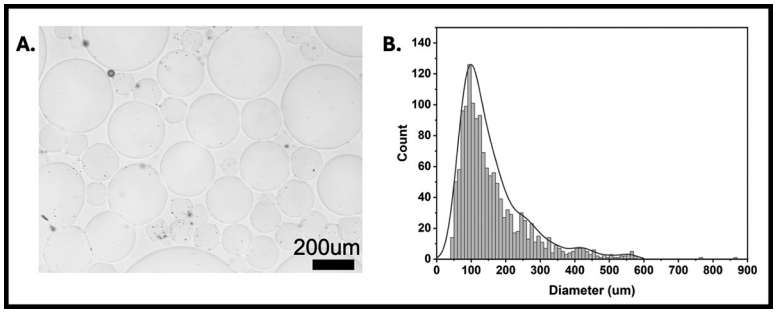

Figure 2: Particle size distributions from batch synthesis. (A) Typical optical images of resulting microgels (Scale bar: 200 µm). (B) Typical size distribution of microgels.

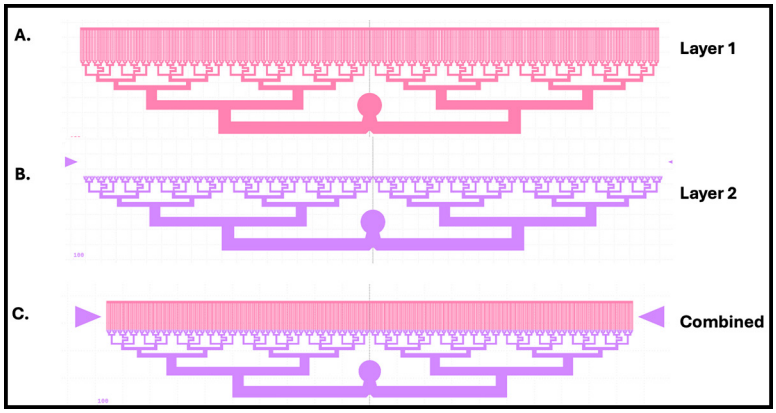

Figure 3: CAD design of the parallel step emulsifier device adapted from the Weitz group [3]. (A) Layer 1; (B) Layer 2; (C) merged images.

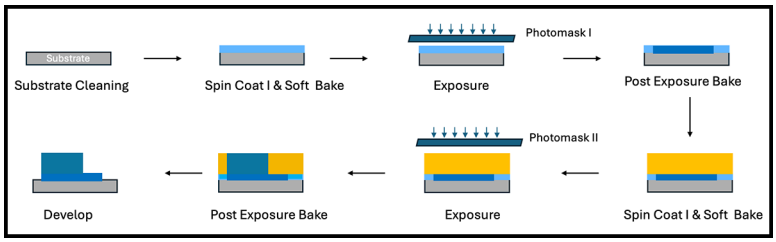

Figure 4: General process flow of the double layer SU-8 master mold fabrication.

Conclusions and Future Steps:

Overall, we synthesized hydrogel particles via inverse suspension polymerization and demonstrated their temperature responsiveness under the microscope. To further understand how individual microgel particles' properties affect the macroscopic rheology properties of the jammed particles, a simple system composed of monodispersed particles was proposed as an alternative. At the CNF, we were able to fabricate an emulsifier device to achieve this goal. In the future, particles with varying compositions will be produced using this device and studied for their rheological behavior.

References:

[1] Oh, K. W.; Lee, K.; Ahn, B.; Furlani, E. P. Design of Pressure-Driven Microfluidic Networks Using Electric Circuit Analogy. Lab Chip 2012, 12 (3), 515–545. https://doi.org/10.1039/c2lc20799k.

[2] Hirotsu S.; Hirokawa, Y.; Tanaka, T. Volume-Phase Transitions of Ionized N-Isopropylacrylamide Gels. Journal of Chemical Physics 1987, 87 (2), 1392–1395. https://doi.org/10.1063/1.453267.

[3] Stolovicki, E.; Ziblat, R.; Weitz, D. A. Throughput Enhancement of Parallel Step Emulsifier Devices by Shear-Free and Efficient Nozzle Clearance. Lab on a Chip 2017, 18 (1), 132–138. https://doi.org/10.1039/C7LC01037k.

Low Loss Superconducting LC Resonator for Strong Coupling with Magnons

CNF Project Number: 2126-12
Principal Investigator(s): Gregory David Fuchs
User(s): Srishti Pal, Qin Xu

Affiliation(s): Department of Applied Physics & Engineering, Department of Physics; Cornell University

Primary Source(s) of Research Funding: Department of Energy (DOE), Center for Molecular Quantum Transduction (CMQT)

Contact: gdf9@cornell.edu, sp2253@cornell.edu, qx85@cornell.edu

Research Group Website: https://fuchs.research.engineering.cornell.edu/

Primary CNF Tools Used: AJA Sputter Deposition, Heidelberg Mask Writer - DWL2000, GCA 6300 DSW 5X g-line Wafer Stepper, YES Asher, PT770 Etcher - Left Side, P7 Profilometer, Zeiss Supra SEM, Nabity Nanometer Pattern Generator System (NPGS), JEOL 6300, Dicing Saw – DISCO, Westbond 7400A Ultrasonic Wire Bonder

Abstract:

We present a hybrid system based on strongly coupled microwave photons hosted by a microstructured resonator and magnon modes of the molecular ferrimagnet vanadium tetracyanoethylene (V[TCNE]x). Using Cornell NanoScale Facility (CNF), we develop a process to integrate the fabrication of high quality-factor (Q-factor) superconducting LC resonators and the deposition of lithographically patterned V[TCNE]x films. We improve the encapsulation of the V[TCNE]x film using atomic layer deposition (ALD) of alumina (Al2O3). We also discuss the design and fabrication of new broadband structures capable of exploring high-power parametric processes in V[TCNE]x films.

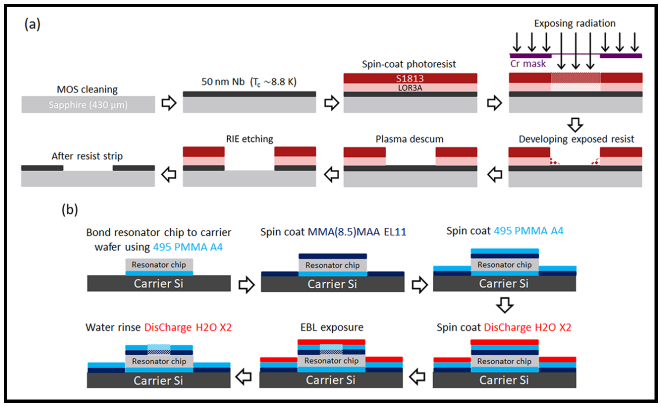

Figure 1: Process flow for (a) patterning the LC resonator using photolithography, and (b) e-beam patterning for V[TCNE]x deposition.

Summary of Research:

This research is focused on studying two systems.

(i) A strongly coupled hybrid photon-magnon system where the coupling strength between the two sub-systems exceeds the mean energy loss in either of them. The key figure-of-merit of this hybrid system is its cooperativity $C=4g^2/k_m k_r$, where g is the coupling strength between magnons and photons, and k_m and k_r are the damping rates for magnons and photons, respectively. The system operates in strong-coupling regime if $C > 1$. (ii) The non-linear excitation of magnons in V[TCNE]x waveguides using high microwave powers.

As a cavity for microwave photons for the coupled photon-magnon system, we use lumped-element planar LC resonators fabricated on superconducting niobium thin-film offering high Q-factor and thus low ..... The basic steps for patterning our LC resonators using photolithography are shown in Figure 1(a).

First, we sputter a 50 nm thick niobium film (thickness measured using P7 profilometer) on a MOS cleaned sapphire substrate using the AJA sputter deposition tool. The superconducting transition temperature (T_c) of our niobium film is ~8.8 K, which is high enough to offer low damping in our operating temperature range of 0.4 - 4 K. The resonator design, patterned on a photomask using Heidelberg Mask Writer-DWL2000, is then cast onto the resist coated wafer (we spin-coat a resist bilayer of LOR3A and S1813) using 5X g-line Wafer Stepper. The developed resist (in AZ726MIF) is descummed in YES Asher followed by dry etching of niobium in PT770.

Finally, we strip the resist in 1165 and dice the wafer using Dicing Saw–DISCO to separate the chips patterned on the wafer. For the magnon sub-system, we use the low-loss organic ferrimagnet V[TCNE]x with a low

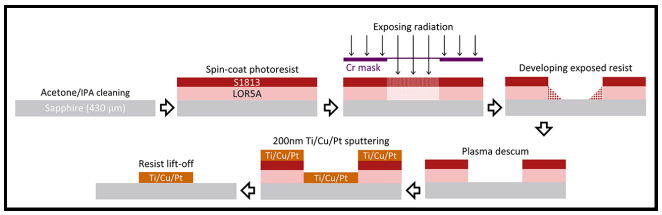

Figure 2: Process flow for fabricating broadband chips with Ti/Cu/Pt tri-layer.

Gilbert damping $\alpha \sim 10^{-4}$ offering long magnon lifetime and thus low k_m Using e-beam lithography in JEOL 6300 or Nabity Nanometer Pattern Generator System (NPGS) connected to Zeiss Supra SEM, we pattern a 6 μm wide and 600 μm long bar on the 10 μm wide and 600 μm long inductor wire using the steps shown in Figure 1(b). We then ship the exposed resonator chips to our collaborators in Ohio State University for V[TCNE]x growth and liftoff.

To avoid saturation of the superconducting niobium film due to formation of vortices at high microwave powers, we chose to fabricate the broadband chips with low resistivity Ti/Cu/Pt tri-layer. The steps for this fabrication are illustrated in Figure 2. First, we coat clean (with acetone followed by IPA) sapphire wafers with bilayer of LOR5A and S1813. The resist coated wafer is then exposed in 5X g-line Wafer Stepper to be patterned with the design written on a photomask using Heidelberg Mask Writer-DWL2000. The developed resist (in AZ726MIF) is descummed in YES Asher followed by deposition of 200 nm thick Ti/Cu/Pt tri-layer in the AJA sputter deposition tool. Finally, we lift-off the resist using 1165 and then dice the wafer using Dicing Saw–DISCO.

The degradation of the organic ferrimagnet V[TCNE]x when exposed to air has necessitated its encapsulation, primarily with epoxy and cover glass as also adopted in our earlier studies [1,2]. Despite offering protection against air exposure, this encapsulation suffers from the demerit of exerting large inhomogeneous strain on V[TCNE]x as the sample is cooled down due to the disparate thermal expansion coefficients of sapphire and epoxy. A solution to this problem is to encapsulate with a material that has a similar thermal expansion coefficient to sapphire, like alumina (Al_2O_3). To test the performance of the hybrid resonator-magnon system with alumina as the encapsulation material, we collaborated with Ohio State University for V[TCNE]x growth and Northwestern University for the atomic layer deposition (ALD) of alumina. Figure 3(a)-(c) showcases the microscope images and the schematic cross-section of the alumina encapsulation on the

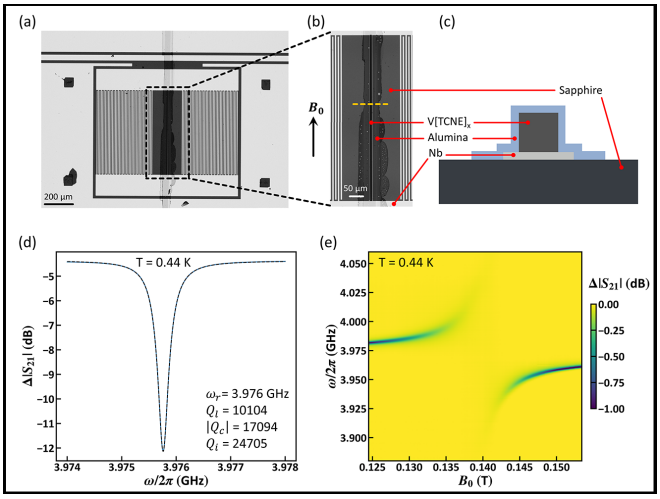

Figure 3: (a) Microscope image of LC resonator device with patterned V[TCNE]x and ALD encapsulation. (b) Magnified microscope image around the region marked with black dashed rectangle in (a). (c) Illustration of the cross section of the device along the yellow dashed line in (b). (d) Fitted (black dashed line) resonator response (blue curve) with extracted Q-factors at 0 T at 0.44 K. (e) 2D colormap of .|S21| as a function of static magnetic field and microwave frequency at 0.44 K.

V[TCNE]x bar grown on the inductor wire of our LC resonator. The fitted resonator response at 0.44 K as shown in Figure 3(d) reveals the internal Q-factor as high as 24705. The anti-crossing obtained for the coupled resonator-magnon system is shown in Figure 3(e). The uniaxial anisotropy field H_k, a quantitative measure of the inhomogeneous strain on the V[TCNE]x, extracted from the anti-crossing turns out to be 6.8 mT which is an order of magnitude lower than that obtained for our previous epoxy encapsulated sample [2].

Conclusions and Future Steps:

We have demonstrated our successful upgradation of the V[TCNE]x encapsulation to reduce the strain and hence the magnetocrystaline anisotropy at the cryogenic temperature. We will integrate the broadband chips with V[TCNE]x encapsulated with alumina to explore high-power non-linear instability processes in V[TCNE]x.

References:

[1] H. F. H. Cheung, et al, "Raman Spectroscopy and Aging of the Low-Loss Ferrimagnet Vanadium Tetracyanoethylene", The Journal of Physical Chemistry C 125, 20380 (2021).

[2] Q. Xu, et al, "Strong Photon-Magnon Coupling Using a Lithographically Defined Organic Ferrimagnet", Advanced Science 11, 2310032 (2024).

Investigation of Dry Chemical Actuators Using Palladium Thin Films

CNF Project Number: 2736-18
Principal Investigator(s): Nicholas Lawrence Abbott[1]
User(s): Hanyu Alice Zhang[2]

Affiliation(s): 1. Chemical and Biomolecular Engineering, 2. Applied and Engineering Physics; Cornell University

Primary Source(s) of Research Funding: Cornell Center for Materials Research with funding from the National Science Foundation Materials Research Science and Engineering Centers program (DMR-1719875)

Contact: nla34@cornell.edu, hz496@cornell.edu

Research Group Website: https://nlabbottcornell.weebly.com/

Primary CNF Tools Used: Heidelberg DWL2000 Mask Writer, ABM Contact Aligner, Oxford 81/82/100 Etchers, AJA Sputter Deposition Tools, Plasma-Therm Takachi HDP-CVD, SC4500 Odd-Hour Evaporator, PT770 Etcher (Left Side), OEM Endeavor Aluminum Nitride Sputtering System, Leica CPD300 Critical Point Dryer, DISCO Dicing Saw

Abstract:

The goal of this work is to design microscale systems that enable the conversion from chemical to mechanical energy via chemomechanical transduction. Previously, by making use of the surface chemistry of platinum, we have demonstrated that a platinum-titanium bimorph can respond to changes in its environment and actuate [1]. In contrast to platinum's surface reactions with gaseous hydrogen and oxygen, palladium is a material known to absorb atomic hydrogen in bulk. In this work, we demonstrate that we can use both surface and bulk properties of palladium to drive actuation.

Summary of Research:

Palladium is well-known for its ability to absorb hydrogen in bulk, thus enabling it to be a material of choice for sensing [2-4], hydrogen purification [2], and storing hydrogen [2,5].

While hydrogen is diffusing into bulk palladium, the material can undergo a phase transition from a hydrogen-poor α phase to a hydrogen-rich β phase depending on the concentration of hydrogen that the palladium is exposed to. The α→β phase transition causes a lattice expansion which can induce a large amount of strain. This is normally undesirable for sensing and storage purposes, however, in this project we present a novel way to utilize this strain to drive microscopic actuators, enabling the development of mechanisms such as small mechanical switches that can not only sense the presence of hydrogen, but also control the amount of hydrogen present by closing and opening a valve.

Figure 1A shows an array of fabricated hinges post release, and Figure 1B shows an individual hinge. To

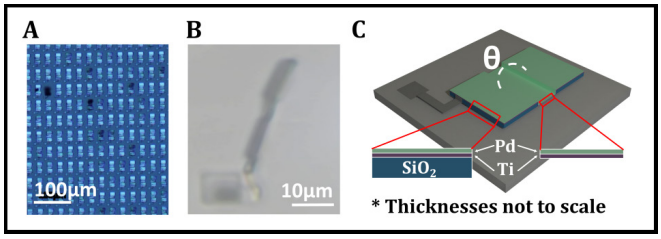

Figure 1: Optical micrographs and 3D rendering of individual hinges.

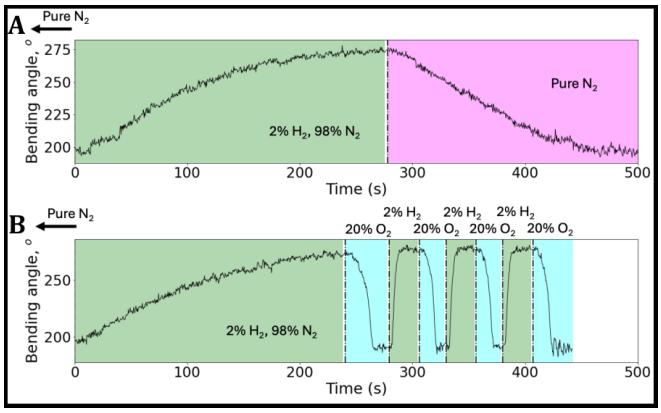

Figure 2: Actuation data upon exposing a hinge to cycling between A) 2 v% H_2 and 20 v% O_2 (All counterbalanced to 1 atm with N_2) and B) 2 v% H_2 and ultra high purity N_2.

fabricate these hinges, a sacrificial layer of aluminum nitride is used, and rigid 600 nm think silicon dioxide panels are deposited on top of the aluminum nitride via chemical vapor deposition. After the rigid panels are patterned, a thin layer of titanium is sputtered to act as a tether, after which the bimorph consisting of 20 nm of sputtered titanium and 20 nm of sputtered palladium is deposited, completing the fabrication process. A 3D

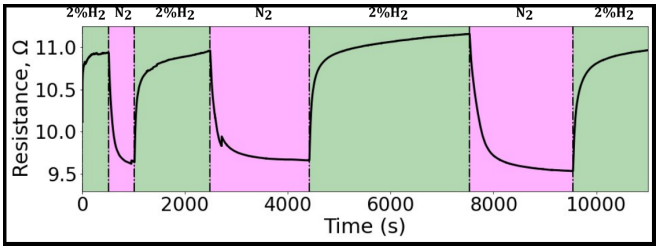

Figure 3: Resistance data upon exposing a palladium film to cycling between 2 v% H2 and ultra high purity N2.

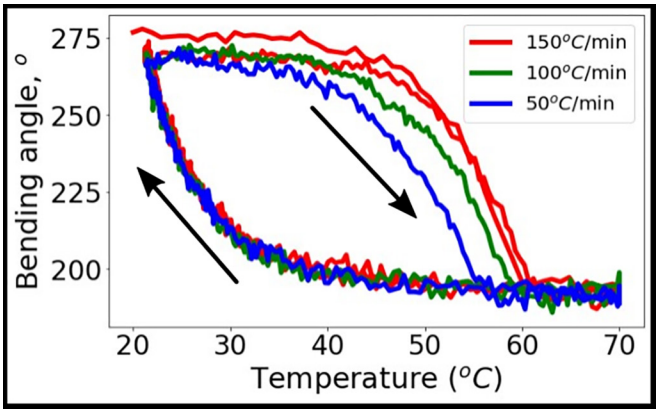

Figure 4: Temperature driven actuation of the palladium hinge under different temperature ramp rates.

rendering of an individual hinge with all the layers is shown in Figure 1C. The chips are then diced, released, dried in the critical point drier, and brought to the lab for experimentation.

Upon exposing the devices to 2 v% H2, 20 v% O2, or ultra pure nitrogen (all at 1 atm, H2 and O2 counter-balanced with N2), we observe an actuation of around 100 .on our 3 μm long hinges, as shown in Figure 2.

We also notice that the application of oxygen instead of nitrogen drives faster actuation not only while oxygen is turned on, but also the oxygen affects the rate of actuation while hydrogen is applied.

We think that actuation in 2 v% H2 and ultra pure nitrogen is driven by the formation of palladium hydride as atomic hydrogen is diffusing into the palladium lattice. Upon the application of oxygen gas to the palladium hydride system, oxygen molecules can dissociate and react with atomic hydrogen in the palladium lattice to form OH. and eventually water. This provides an additional chemical pathway for atomic hydrogen to be removed from the palladium lattice.

To test the formation of palladium hydride, we have conducted additional experiments via the measurement of electrical resistance, as shown in Figure 3.

In addition, because the formation of palladium hydride is known to be a temperature-dependent process, we were able to show that we can drive a similar actuation by cycling the temperature in a 2 v% H2 environment.

Conclusions and Future Steps:

Through numerous analyses and fabrication runs, we have shown that the devices actuate reliably and reproducibly. We are currently in the process of understanding the material science and chemistry behind these actuators and running experiments to test our theoretical models and hypotheses.

References:

[1] N. Bao, et al. Gas-phase microactuation using kinetically controlled surface states of ultra-thin catalytic sheets. PNAS, 120(19), 2023.

[2] B.D. Adams and A, Chen. The role of palladium in a hydrogen economy. Materials Today, 14(6):282-289, 2011.

[3] I. Darmadi, F. A. A. Nugroho, and C. Langhammer. High-performance nanostructured palladium-based hydrogen sensors—current limitations and strategies for their mitigation. ACS sensors, 5(11):3306-3327, 2020.

[4] C. C. Ndaya, N. Javahiraly, and A. Brioude. Recent advances in palladium nanoparticles-based hydrogen sensors for leak detection. Sensors, 19(20):4478, 2019.

[5] S. K. Konda and A. Chen. Palladium based nanomaterials for enhanced hydrogen spillover and storage. Materials Today, 19(2):100-108, 2016.

Metal-Organic Framework-Inspired Metal-Containing Clusters for High-Resolution Patterning

CNF Project Number: 2751-18
Principal Investigator(s): Christopher Kemper Ober
User(s): Emma Hester

Affiliations(s): Department of Materials Science and Engineering, Cornell University

Primary Source(s) of Research Funding: Office of Naval Research (ONR)

Contact: cko3@cornell.edu, egh66@cornell.edu

Research Group Website: https://ober.mse.cornell.edu/index.html

Primary CNF Tools Used: Molecular Vapor Deposition (MVD), Atomic Force Microscope (AFM)

Abstract:

In order to treat surfaces for resistance of a wide range of marine organisms, surface chemistry, physical properties, durability, and attachment scheme must all be considered in the synthesis and design of a coating. By synthesizing a hydrophobic polymer backbone and modifying it to contain different functional groups with varying degrees of hydrophilicity, it is possible to achieve an overall amphiphilic material that is resistant to settlement and will promote removal of certain marine species. Surface characterization of these thin films suggests that buffered and zwitterionic species are capable of interfering with calcareous and non-calcareous foulers.

Summary of Research:

PS-PVMS is a block copolymer that was synthesized to high purity using a method previously established by the Ober group [1]. The polymer contains a vinyl group that is reactive and is later utilized in thiol-ene click chemistry in order to attach different chemical functionalities that are thought to be useful in generating antifouling and foul resistant surfaces. The following buffers were synthesized (Figure 1) with corresponding water contact angles. Generally speaking, the goal is to have more hydrophilic character as most foulers are more attracted to hydrophobic materials. In this case, however, it was found that the more hydrophobic materials better resisted fouling.

The process of coating the slides starts with molecular vapor deposition of a thin single layer of APTMS on piranha cleaned slides. This prepares the substrate for the following layers: Ma-SEBS, SEBS, and finally, the PS-PVMS modified antifouling coating. (Figure 2). With the addition of each layer, water contact angle is once again measured prior to addition of the following layer. Ma-SEBS and SEBS are thermally annealed to the surface post drying in a 120°C oven for 12 hours, which helps with thermal stability and increases the durability of the materials in the water. The final layer is then spray coated on to the surface. Synthetic methods adapted from [2-4].

AFM was used to characterize the surface morphology of each of the coatings. AFM gave a better idea of the uniformity of the coatings (Figure 3). In the images it was noted that ImZ-PVMS had some crater-like formations. It is not totally clear what caused this, but it is important to note as this can impact the results of fouling. One theory is that because the permanent zwitterionic imidazole group contains two opposite charges within a close proximity to one another, it is possible that intermolecular entanglement becomes higher resulting in an overall rougher surface [5].

References:

[1] Zhang, Z.; Chaudhuri, K.; Kaefer, F.; Malanoski, A. P.; Page, K. A.; Smieska, L. M.; Pham, J. T.; Ober, C. K. Controlling Anti-Penetration Performance by Post-Grafting of Fluorinated Alkyl Chains onto Polystyrene-block-poly(vinyl methyl siloxane). ACS Applied Materials and Interfaces 2024, 16(15).

[2] Leonardi, A. K.; Medhi, R.; Zhang, A.; Düzen, N.; Finlay, J. A.; Clarke, J. L.; Clare, A. S.; Ober, C. K. Investigation of N-Substituted Morpholine Structures in an Amphiphilic PDMS-Based Antifouling and Fouling-Release Coating. Biomacromolecules 2022, 23, 2697–2712.

[3] Leonardi, A. K.; Ober, C. K. Polymer-Based Marine Antifouling and Fouling Release Surfaces: Strategies for Synthesis and Modification. Annu. Rev. Chem. Biomol. Eng. 2019, 10, 241–264.

[4] Leonardi, A. K.; Zhang, C; Düzen, N.; Aldred, N.; Finlay, J. A.; Clarke, J. A.; Clare, A. S.; Segalman, R.; Ober, C. K. "Amphiphilic nitroxide bearing siloxane-based block copolymer coatings for enhanced marine fouling release", Appl. Mater. Int., (2021), 13(24), 28790-28801

[5] Lin, C. H.; Luo, S. C. Zwitterionic Conducting Polymers: From Molecular Design, Surface Modification, and Interfacial Phenomenon to Biomedical Applications. Langmuir 2022, 38(24), 7383-7399.

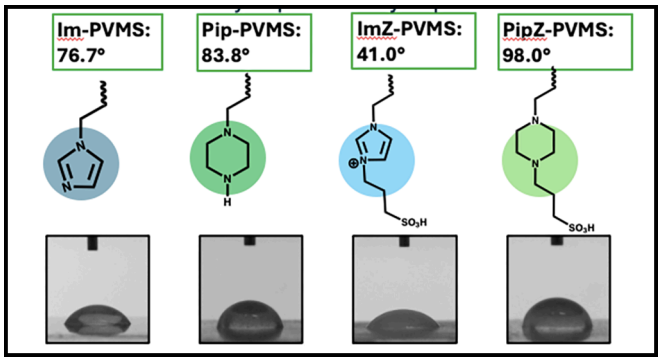

Figure 1: Four buffers were synthesized and attached to a PS-PVMS backbone via thiol-ene click chemistry. Once adhered, corresponding water contact angles were measured to gauge effectiveness of reaction and to test surface presence.

Image Depiction of Layer	Chemical Identification	Water contact angle
	Piranha cleaned slides	4.7±0.9 °
	APTMS	45.9±3.5°
	Ma-SEBS	97.8±1.1°
=SEBS	SEBS	99.6±2.4°

Figure 2: Visual depiction of each layer and water contact angles post adhesion/thermal annealing.

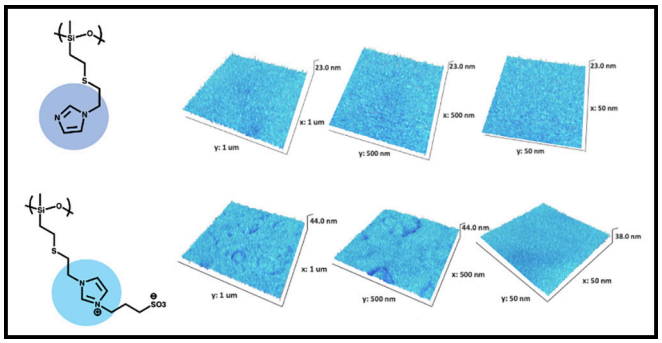

Figure 3: Imidazole family of buffered PS-PVMS AFM surface characterization.

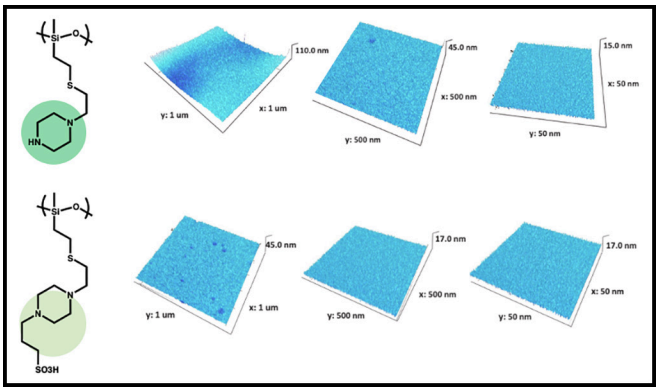

Figure 4: Piperazine family of buffered PS-PVMS AFM surface characterization.

Thiol-Norbornene Photopolymer for Two-Photon Photopolymerization

CNF Project Number: 2754-18
Principal Investigator(s): Yadong Wang
User(s): Warrick Ma

Affiliation(s): Chemistry and Chemical Biology, Cornell University

Primary Source(s) of Research Funding: Cornell Startup Fund; Ignite Innovation Acceleration Grant

Contact: yw839@cornell.edu, ym464@cornell.edu

Research Group Website: https://biofoundry.bme.cornell.edu

Primary CNF Tools Used: Nanoscribe Photonic Professional GT2 Two-Photon Lithography System

Abstract:

Carbic anhydride is an underappreciated starting material for 3D-printable, non-hydrogel photopolymers. Compared with other norbornene precursors, carbic anhydride is cheaper and reactive via aminolysis. As a result, the generalized and efficient functionalization with carbic anhydride can increase the utilization of thiol-norbornene photopolymers. Here, we report carbic anhydride's catalyst-free condensation with two commodity polymers: amine-functionalized polypropylene glycol and polydimethylsiloxane. The reaction completes in 1h, produces water as the only byproduct, and does not require purification. It is therefore affordable, facile, and green. Mixing the product with thiol cross-linkers and the appropriate photo-additives produces photopolymers, which have the potential to be used for microfabrication with two-photon photopolymerization (2PP). The simple yet versatile platform will benefit additive manufacturing of soft materials and beyond.

Summary of Research:

Thiol-norbornene photopolymers are excellent for additive manufacturing. Nevertheless, scalable thiol-norbornene photopolymers need a more affordable starting material and a more scalable synthesis. Among the norbornene precursors, carbic anhydride (CA) is the cheapest and greenest. CA reacts via alcoholysis or aminolysis, thermodynamically favorable processes that can occur without a catalyst. If water is removed from the reaction mixture, CA's reaction with amine yields norbornene dicarboximide [1-3]. Adapting this strategy will make the synthesis of thiol-norbornene photopolymers greener and more economical.

The norbornene dicarboximide-functionalized polymers are synthesized from amine-functionalized PPG and PDMS (Figure 1). Proton nuclear magnetic resonance (1H-NMR) indicates the clean formation of norbornene dicarboximide from the singlet at 6.0-6.1 ppm (Figure 2). Except for 7kPDMS-5CA, all products are transparent liquids. 7kPDMS-5CA's opacity potentially arises from the partial crystallinity of the pendant norbornene dicarboximide propyl side chains.

Two thiol cross-linkers, pentaerythritol tetrakis(3-mercaptopropionate) (PETMP) and 4.6% (mercaptopropyl)methylsiloxane]-dimethylsiloxane copolymer (polySH), are used to study photopolymerization. PETMP is miscible with PPG-based polymers but not with PDMS-based polymers. As a result, 0.9kPDMS-2CA:PETMP is a milky-white mixture. We attempted to solubilize PDMS-based polymers with polySH. However, only 5kPDMS-2CA:polySH is transparent. All immiscible mixtures remain stable emulsions after overnight storage without agitation. Aggregate formation may lead to a heterogeneous network and affect the mechanical properties of 3D-printed materials [4].

To assess the printability of norbornene dicarboximide photopolymers, we investigated their photorheology with 400-500 nm light to capture the effect of 2PP cross-linking. Judging by the cross-over point of loss and storage modulus, only 5kPPG-3CA:PETMP cross-links too slowly (385 nm or 405 nm). Cross-linked 5kPPG-3CA:PETMP is also extremely soft and tacky, indicative of a weak network not suitable for additive manufacturing. All other photopolymers cross-link quickly, with various cross-over points (Figure 3) reflecting the structure-property relationships.

After rheological studies identified four printable formulations, they were tested for 2PP. PDMS-based photopolymers are unsuitable for 2PP due to light scattering resulting from the heterogeneous mixture. 2kPPG-2CA:PETMP shows the best solubility in isopropyl alcohol, and thus is used as a proof-of-concept for 2PP (Figure 4). The cured photopolymer in the camera view suggests the photopolymer's feasibility.

The catalyst-free condensation between amine-functionalized PPG or PDMS and CA affords a family of

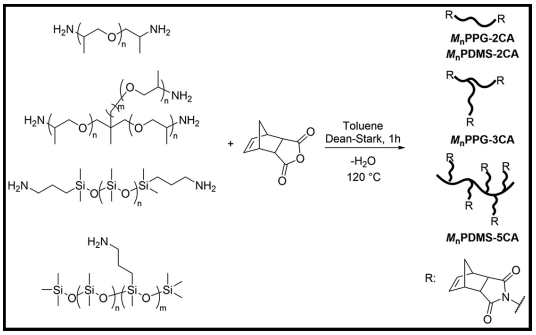

Figure 1: Synthesis of norbornene dicarboximide polymers from amine-functionalized polypropylene glycol (PPG) or polydimethylsiloxane (PDMS). The prefix Mn represents the average molecular weight of the amine-functionalized starting material. The number preceding CA represents the number of norbornene dicarboximide groups in a single chain. For example, amine-terminated PPG (Mn = 2 kDa) affords 2kPPG-2CA.

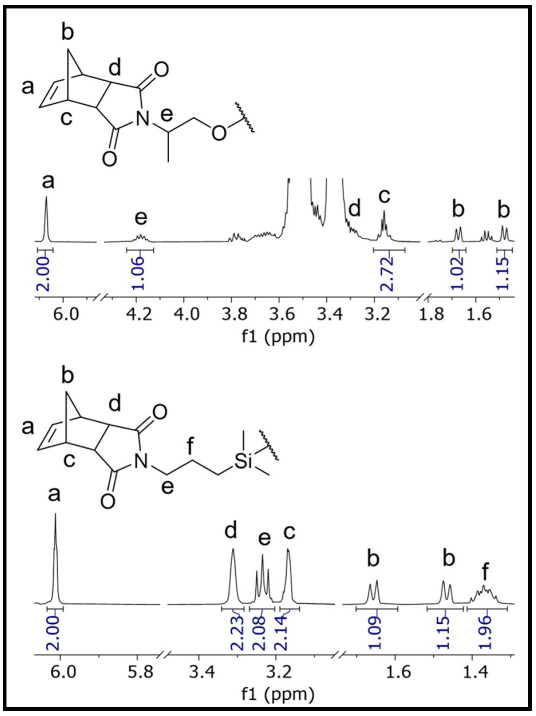

Figure 2: 1H-NMR spectra of norbornene dicarboximide-functionalized polymers showing their end group structure (500 MHz, CDCl3).

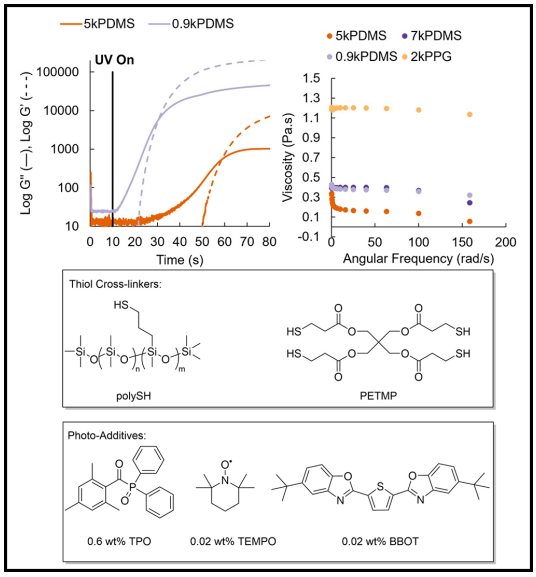

Figure 3: Photorheology and viscosity of representative photopolymers (names are abbreviated to their respective backbone). The photorheology data of 2kPPG and 7kPDMS are in Figure S3. Ultraviolet (UV) radiation (400-500 nm, 10 mW/cm^2) is switched on at 10 s (G': storage modulus; G" loss modulus).

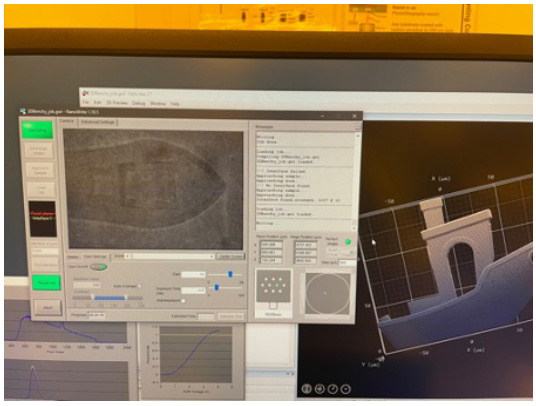

Figure 4: 2PP on Nanoscribe Photonic Professional GT2 Two-photon Lithography System with 2kPPG-2CA:PETMP showing cured 3D object on the substrate. Solvent washing during post-printing obliterated the object, potentially due to rapid solvent swelling of the partially cured photopolymer.

norbornene dicarboximide functionalized polymers—with water as the only byproduct. The reaction is affordable and green and occurs at a 100-g scale without purification. The resultant photopolymers have potential in microfabrication with 2PP. Cheap but versatile, our method can benefit additive manufacturing of soft materials and beyond. In the future, the 2PP parameter should be systematically fine-tuned for successful fabrication.

References:

[1] Wang, H., et al. Polym Chem-Uk 2024, 15 (6), 534-543. DOI: 10.1039/d3py01278f.

[2] Majchrzak, M., et al. Polymer 2012, 53 (23), 5251-5257. DOI: 10.1016/j.polymer.2012.09.033.

[3] Pawloski, A. R., et al. J Photopolym Sci Tec 2002, 15 (5), 731-739. DOI: DOI 10.2494/photopolymer.15.731.

[4] Abdilla, A., et al. J Polym Sci 2021, 59 (19), 2114-2128. DOI: 10.1002/pol.20210453.

Influence of Ligand for Metallo-Elastomer Design

CNF Project Number: 2754-18
Principal Investigator(s): Yadong Wang
User(s): Chia-Wei Yeh, Simon Van Herck

Affiliation(s): Biomedical Engineering, Cornell University

Primary Source(s) of Research Funding: NIH

Contact: yw839@cornell.edu, cy465@cornell.edu, sbv25@cornell.edu

Research Group Website: https://biofoundry.bme.cornell.edu/

Primary CNF Tools Used: Rame-Hart 500 Goniometer

Abstract:

Metal-ligand coordination is an appealing strategy pursued to achieve crosslinking in the design of elastomers for biomedical applications. A variety of ligands, like catechols and imidazole groups, can be employed to achieve this and have been reported in literature. However, material property comparisons are usually done on a single ligand with variations in ligand density or complexation metal. Here, we intend to expand our understanding of ligand-metal coordination crosslinking in elastomer design via a head-to-head comparison of different ligands. We designed a modular polymer platform that allowed for easy conjugation with a Salen-, pyridoxal- or catechol based ligand. These polymers are used to evaluate the influence of the ligand on chelation strength, mechanical properties, catalytic activity and biological interaction.

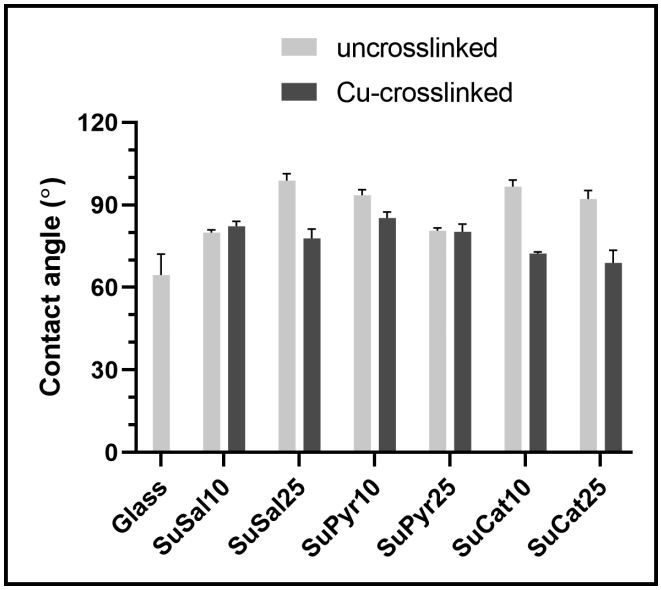

Figure 1: Plot of contact angles of water droplet on polymer surface for polymer only (= no Cu) and Cu-crosslinked polymer films.

Summary of Research:

The experimental work done in collaboration with CNF for this project is limited to contact angle measurements, using the Rame-Hart 500 Goniometer.

Thin films were prepared of polymer only or polymer crosslinked with Cu-salts on glass slides. The contact angle between a water droplet and the hydrophobic surface was analyzed. Overall, we observed a clear trend with a decrease in contact angle for films crosslinked with Cu compared to uncrosslinked films, indicating a more hydrophilic surface. We hypothesize that this is due to the crosslinking chemistry of these ligands that occurs via the formation of a phenolate anion that will chelate with the Cu-ion, the thereby generated ionic content increased hydrophilicity. This hypothesis is supported by the largest decrease for catechol (SuCat10 and SuCat25) based polymer due to deprotonation of both phenolic protons and higher anionic surface. An overview of the results is given in Figure 1 and 2.

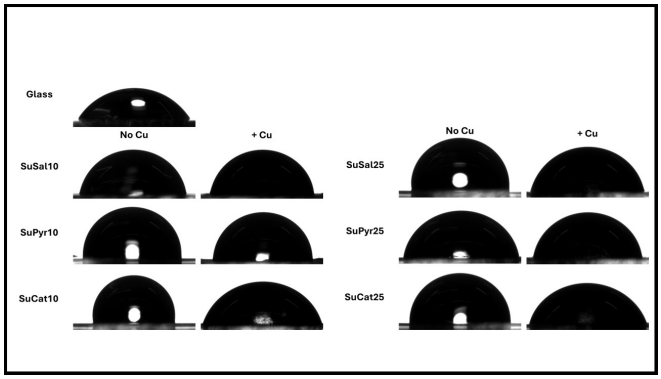

Figure 2: Visual presentation of change in contact angle upon Cu-crosslinking of films.

Fabrication of Polymer Grafted Core-Shell Nanoparticles

CNF Project Number: 2955-21
Principal Investigator(s): Christopher Ober
User(s): Yu Shao

Affiliation(s): Materials Science and Engineering, Cornell University

Primary Source(s) of Research Funding: NSF

Contact: cko3@cornell.edu, ys2295@cornell.edu

Primary CNF Tools Used: Zetasizer

Abstract:

Polymer-grafted nanoparticles (PGNs) possess the advantages of both polymers and inorganic cores, and demonstrate superior magnetic, optical, electronic, and mechanical properties. PGNs were synthesized by mini-emulsion polymerization and the brush canopy size, graft density and molar mass of the grafted polymer chains could be controlled by modifying the monomer feeding rate, the monomer concentration, and other parameters. Through combined technologies we are about to fabricate a series of inorganic-inorganic core-shell nanoparticles based on unique silicon-containing polymer precursor and unfold the structure-property relationship towards cutting edge magnetic and photoresponsive materials.

Summary of Research:

In this research, it is critically important to obtain stable colloidal emulsion systems that create a nano-encapsulation environment and then be able to graft uniform polymer brushes on the surface of NPs. To characterize the colloidal suspension, we use mainly dynamic light scattering (DLS) technique to monitor the emulsion condition before and after polymerization. As shown in Figure 1, particle size and distribution can be varied due to different monomer feeding ratio. Morphology of core-shell NPs is uniform with PDI close to 0.1 according to DLS and also confirmed by STEM (Figure 2). However, when it comes to preceramic polymer coating, it's tricky to make a uniform emulsion system.

As shown in Figure 3, even though the data file says good quality, the curve shows an asymmetric peak profile which means that the size distribution is not uniform. In addition, concentration and temperature will influence the colloidal system a lot. Progress needs more of modification.

Conclusions and Future Steps:

DLS is a facile tool to characterize the emulsion condition of colloidal system. For emulsions with nanoparticles and multiple ingredients, it's a challenge to make ideally uniform nano-encapsulation environments. Concentration and temperature play critical roles and need to be modified systematically in the future.

References:

[1] Chenyun Yuan, Florian Kafer, and Christopher K. Ober. (2021). Polymer-Grafted Nanoparticles (PGNs) with Adjustable Graft-Density and Interparticle Hydrogen Bonding Interaction.

[2] Alicia Cintora, Florian Kafer, Chenyun Yuan, and Christopher K. Ober. (2021). Effect of monomer hydrophilicity on ARGET-ATRP kinetics in aqueous mini-emulsion polymerization.

[3] Roselynn Cordero, Ali Jawaid, Ming-Siao Hsiao, Zoe Lequeux, Richard A. Vaia, Christopher K. Ober, "Mini Monomer Encapsulated Emulsion Polymerization of PMMA in Aqueous ARGET ATRP", ACS Macro Letters, 7, 4, 459-463.

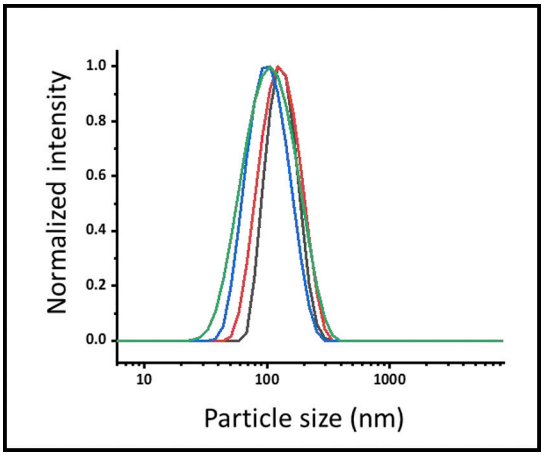

Figure 1: DLS overlay of CdS nanoparticles coated with silica shell.

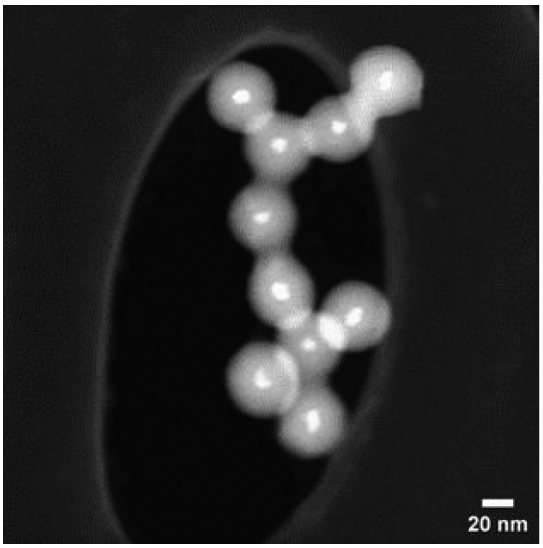

Figure 2: STEM image of CdS nanoparticles coated with silica shell.

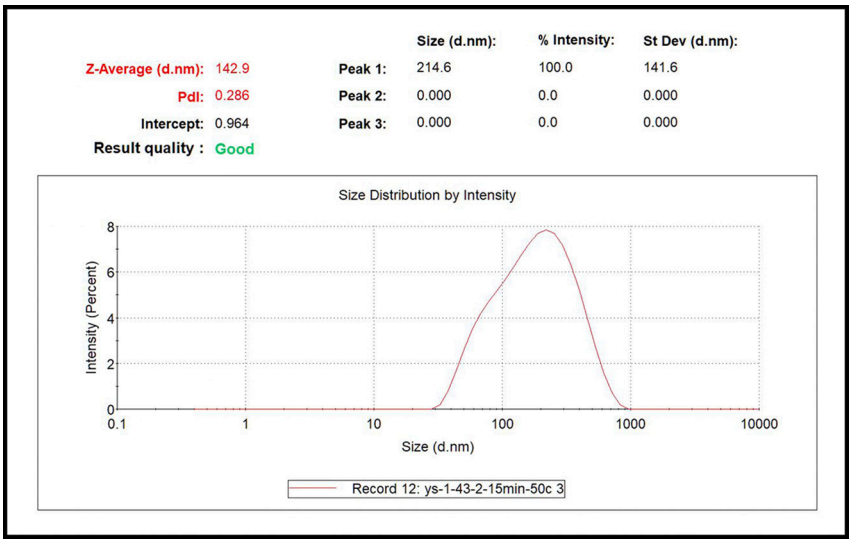

Figure 3: DLS of emulsion made by $CoFe_2O_4$ NPs and preceramic precursors at 50°C.

Quasi-2D Materials for Ultra-Low Resistance Electrical Interconnects

CNF Project Number: 3007-22
Principal Investigator(s): Hair P. Nair
User(s): Bilal Azhar

Affiliation(s): Department of Materials Science and Engineering, Cornell University

Primary Source(s) of Research Funding: Semiconductor Research Corporation (SRC)

Contact: hn277@cornell.edu, ba428@cornell.edu

Primary CNF Tools Used: General Materials Anneal Furnace, Veeco Savannah ALD, Woollam RC2 Spectroscopic Ellipsometer, AJA Sputter Deposition, ABM Contact Aligner, GCA AutoStep 200 DSW i-Line Wafer Stepper, Heidelberg Mask Writer, YES Vapor Prime Oven, AJA Ion Mill, Glen 1000 Resist Strip, Dektak XT Profilometer, Zeiss Ultra SEM

Abstract:

The dramatic increase in the resistivity of interconnect lines with decreasing dimensions presents a significant bottleneck for further downscaling of integrated circuits [1]. This is because current interconnects use 3-dimensional metals that experience increased interface electron scattering as the interconnect dimensions approach their electron mean free path. A possible solution is to use metals with much lower electron mean free paths such as: W, Mo, and Ru. Metallic delafossite oxides are an alternative solution because of their inherent advantages over traditional metals such as: ultra-low room temperature resistivity, potential mitigation of interface/surface scattering due to their 2D Fermi surface, potentially decreased likelihood of electromigration, and potentially better compatibility with low-K oxide dielectrics. Metallic delafossite can prove to be a disruptive new material for ultra-scaled electrical interconnects.

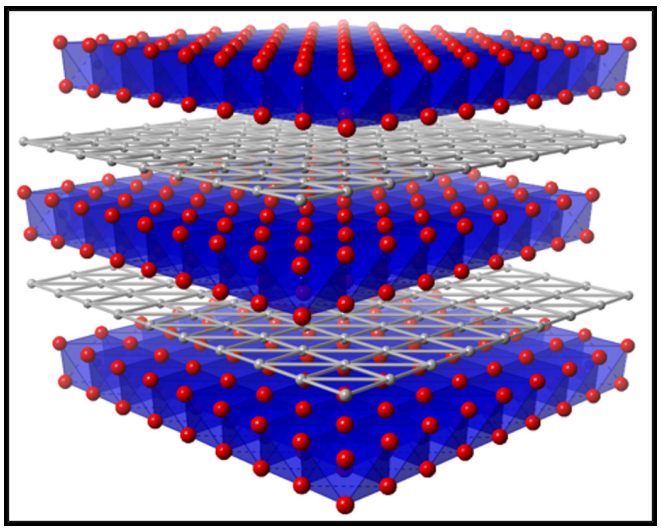

Figure 1: Layered crystal structure of delafossite PtCoO2.

Delafossites are layered oxides with the formula ABO2 where A is a metal cation that forms 2D sheets separated by the BO2 transition-metal oxide octahedra, Figure 1. In this study we focus on metallic delafossites PtCoO2 and PdCoO2 because of their ultra-low room temperature resistivity of 2.1 $\mu\Omega$.cm and 2.6 $\mu\Omega$.cm, respectively, which is comparable to the current semiconductor industry standard interconnect metal, Cu, Figure 2 [2]. The metallic delafossite structure has an anisotropic nature with resistivity along the c-axis a factor of 500 higher than resistivity within the Pt/Pd sheet. Due to the layered crystal structure, the Fermi surface of the metallic delafossites is cylindrical as for a 2D metal. This quasi-2D crystal structure can potentially mitigate interface and surface scattering since the electron Fermi velocity does not have components perpendicular to the Pd/Pt sheets. This can potentially overcome the resistivity penalty encountered by conventional 3D metals in ultrathin films (< 20 nm). Additionally, the unique Fermi surface topology allows for an electron-phonon coupling constant that is a factor of 3 lower than copper [3].

Our focus has been to demonstrate metallic delafossites as a disruptive new material for ultra-scaled electrical interconnects, for which we have two goals. The first goal is to realize their unique electrical properties and the second goal is to demonstrate the growth of highly quality delafossite thin films via atomic layer deposition (ALD) a back-end-of-the-line (BEOL) compatible synthesis technique.

Summary of Research:

To realize the unique electrical properties of delafossite thin films we have been investigating the structural and electrical properties of PdCoO2 thin films grown via molecular beam epitaxy (MBE). MBE has been shown to achieve highly crystalline films which is critical for electrical property characterization due to the structure-property relation [4,5]. We used high-resolution X-Ray diffraction (HRXRD) to confirm that the films are phase-pure. We measured the resistivity of the films using a van der Pauw geometry and modelled the resistivity scaling with film thickness using Fuchs-Sondheimer (FS) and Mayadas-Shatzkes (MS) model. The upshot being that a 50 nm thick PdCoO2 film has a resistivity of ~8 $\mu\Omega$.cm. It should be noted that while our XRD phi scans did reveal in-plane twinning our resistivity fitting did not find twin boundaries to be a significant contributor to resistivity.

In addition to modeling the resistivity scaling with thickness, we are also modeling the line-width resistivity scaling into the sub 100 nanometer regime. Towards this we have fabricated micron wide wires via the contact aligner and are fabricating sub-micron wires via the i-line stepper. It is important to scale down incrementally so to check for any lithography-related degradation of the delafossite wires which would make it difficult to isolate the dimension dependent resistivity change.

We are also investigating back-end-of-the-line (BEOL) compatible growth of these materials via Atomic Layer Deposition (ALD) and Sputtering. To guide this effort we have created a thermodynamic model of the PdCoO2 system and are validating it via ex-situ anneals in relevant ambients, temperatures, and time scales to find BEOL conditions in which these materials are stable.

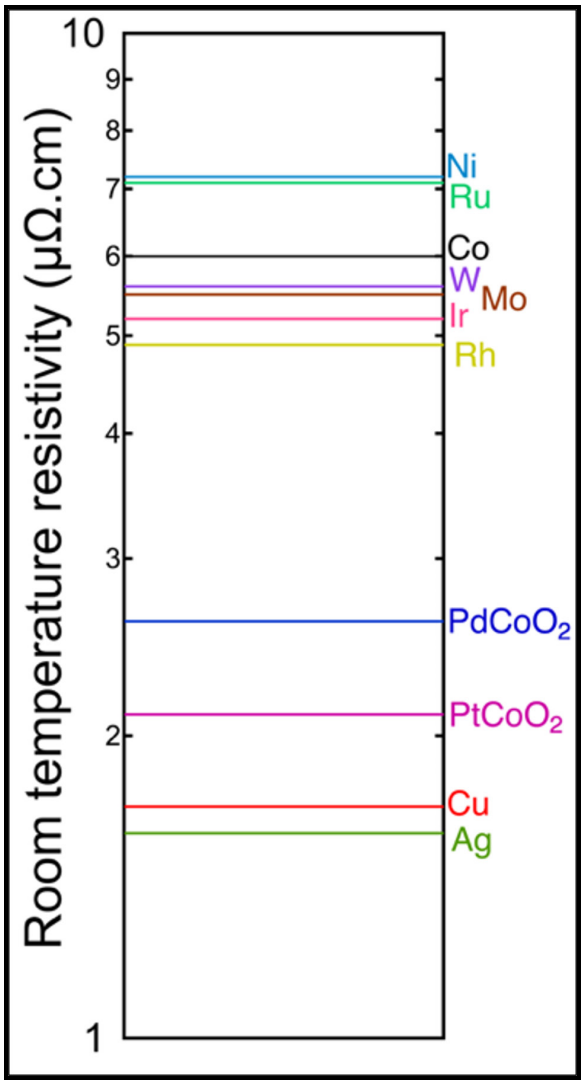

Figure 2: Comparison of room temperature resistivity of $PdCoO_2$ and $PtCoO_2$ to conventional interconnect metals.

Conclusions and Future Steps:

We have three main goals: (1) Characterize the line-width resistivity scaling of these delafossite materials, (2) map out their stability in BEOL conditions, and (3) find a BEOL compatible growth method.

References:

[1] D. Gall, J. Appl. Phys. 127, 050901 (2020).

[2] V. Sunko, P.H. McGuinness, C.S. Chang, E. Zhakina, S. Khim, C.E. Dreyer, M. Konczykowski, M. König, D.A. Muller, and A.P. Mackenzie, Phys. Rev. X 10, 021018 (2020).

[3] C.W. Hicks, A.S. Gibbs, A.P. Mackenzie, H. Takatsu, Y. Maeno, and E.A. Yelland, Phys. Rev. Lett. 109, 116401 (2012).

[4] J. Sun, M.R. Barone, C.S. Chang, M.E. Holtz, H. Paik, J. Schubert, D.A. Muller, and D.G. Schlom, APL Mater. 7, 121112 (2019).

[5] Q. Song, J. Sun, C.T. Parzyck, L. Miao, Q. Xu, F.V.E. Hensling, M.R. Barone, C. Hu, J. Kim, B.D. Faeth, H. Paik, P.D.C. King, K.M. Shen, and D.G. Schlom, APL Mater. 10, 091113 (2022).

Lithiation Induced Phases in 1T.-$MoTe_2$ Nanoflakes

CNF Project Number: 3035-22
Principal Investigator(s): Jeeyoung Judy Cha
Users(s): Natalie Williams, Sihun Lee

Affiliations(s): Materials Science and Engineering, Chemistry and Chemical Biology; Cornell University

Primary Source(s) of Research Funding: The Gordon and Betty Moore Foundation's EpiQS Initiative #9062.01, The National Science Foundation, CBET-CAREER #2240944

Contact: jc476@cornell.edu, nlw49@cornell.edu, sl2859@cornell.edu

Research Group Website: cha.mse.cornell.edu

Primary CNF Tools Used: Heidelberg Mask Writer - DWL2000, SC4500 Odd-Hour & Even-Hour Evaporator

Abstract:

Molybdenum ditelluride (MoTe2) is a layered, two-dimensional (2D) crystal that naturally exists in three different structural phases. Each phase exhibits distinct optical and electronic properties. One way to induce new phases in 2D materials is through the reversible insertion of ions, atoms, or molecules into the gaps of crystalline materials, otherwise known as intercalation. Here we report electrochemical intercalation of lithium (Li) into the distorted octahedral or 1T'-phase of MoTe2 nanoflakes, leading to the discovery of two previously unreported lithiated phases [1].

Summary of Research:

We assembled coin-type cells with 1T'-MoTe2 powder to induce two, distinct and reversible phase transitions upon lithium intercalation. These phases are denoted as lightly lithiated phase I and heavily lithiated phase II (Figure 1). We also fabricated electrochemical cells on individual nanodevices using exfoliated crystals (Figure 2), which allowed for investigations into structure and electrochemical property changes in situ as we directly control intercalation of lithium ions into the 2D crystal. Structural differences between the 1T' and lithiated phase of MoTe2 were characterized by in situ Raman spectroscopy, and a change from the previously metallic to semiconducting phase upon lithiation was revealed through in situ transport measurements (Figure 3). In situ Hall measurements indicated bandgap opening in the lithiated phases, as evidenced by a significantly reduced Hall carrier density, and increasing resistance with decreasing temperature. Changes in structure for the heavily lithiated phase II was further analyzed using in situ angle-resolved Raman spectroscopy, in situ single-crystal x-ray diffraction (XRD), and in situ transition electron microscopy (TEM).

Conclusions and Future Steps:

Successful application of in situ experiments enabled detailed investigations of crystal structure and electronic properties of MoTe2 nanoflakes during electrochemical lithium intercalation. The discovery of new phases in initially metallic 1T'-MoTe2 highlights the effectiveness of electrochemical intercalation in adjusting phase stability and electron density in 2D materials.

References:

[1] S. Xu, K. Evans-Lutterodt, S. Li, N. L. Williams, B. Hou, J. J. Huang, M. G. Boebinger, S. Lee, M. Wang, A. Singer, P. Guo, D. Y. Qiu, and J. J. Cha, Lithiation Induced Phases in 1T'-MoTe2 Nanoflakes, DOI: 10.1021/acsnano.4c06330.

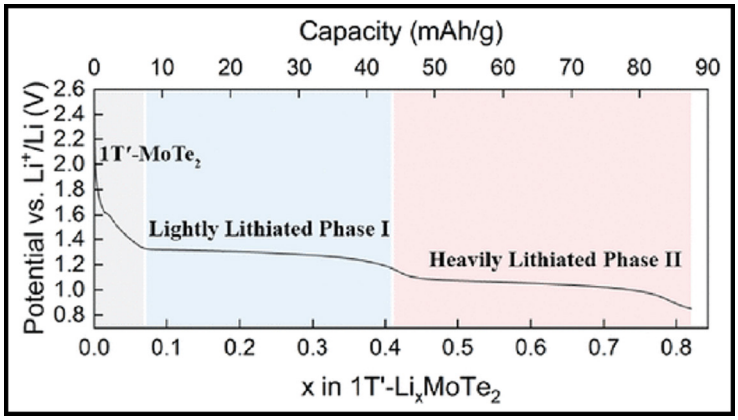

Figure 1: Galvanostatic discharging of 1T'-MoTe2 powder in a coin cell showing two distinct, intermediate phases upon 1T'-MoTe2 lithiation.

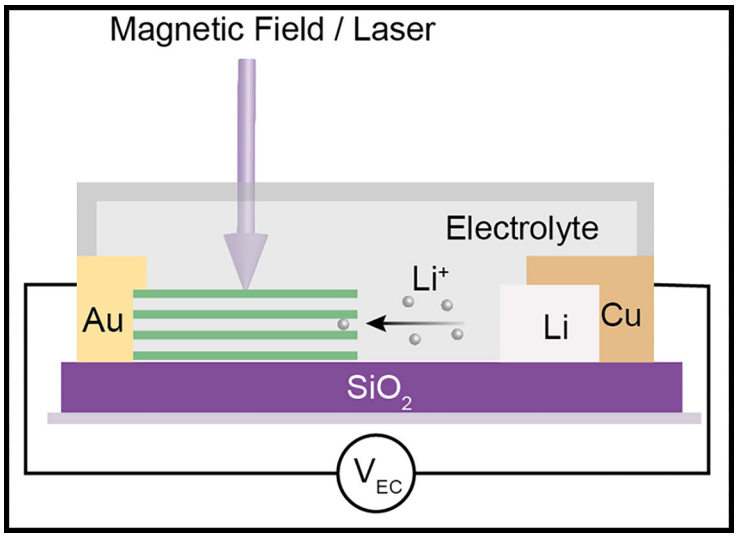

Figure 2: A schematic of a planar electrochemical intercalation cell capable of in situ experiments, such as for Raman spectroscopy, single-crystal XRD, and transport measurements.

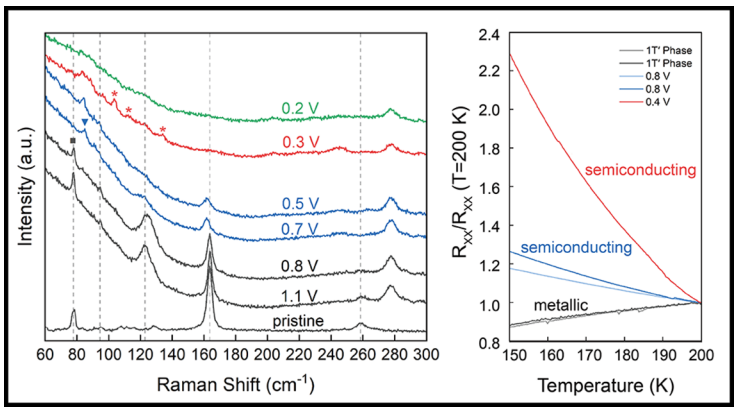

Figure 3: (Left) New structures of lithium intercalated 1T'-MoTe2, namely lightly lithiated phase I and heavily lithiated phase II. (Right) Initially metallic 1T'-MoTe2 is transformed into lithiated, semiconducting phases as confirmed by transport measurements, showing increasing resistance with decreasing temperature.

Measuring Microplastic Migration Through Human Intestinal Mucus

CNF Project Number: 3058-23
Principal Investigator(s): Meredith Silberstein
User(s): Max Tepermeister, Ellen van Wijngaarden

Affiliation(s): Sibley School of Mechanical and Aerospace Engineering, Cornell University

Primary Source(s) of Research Funding: College of Engineering Sprout Award

Contact: meredith.silberstein@cornell.edu, mt845@cornell.edu, ewv8@cornell.edu

Research Group Website: silbersteinlab.com

Primary CNF Tools Used: Harrick Plasma Generator, Malvern Nano ZS Zetasizer

Abstract:

Microplastic accumulation in the body has become a growing concern due to widespread harmful physiological effects. This research is focused on understanding how the intestinal mucus layer prevents the migration of ingested microplastics. We studied how size and surface charge of microplastics of different compositions, functionalization and size alter particle movement through mucus. Previous studies have used alternative mucus models such as porcine gastric mucus and have focused primarily on one plastic composition. Our study uses mucus derived from a human colonic cancer cell line, HT29MTX, and tests a broad range of plastic compositions and sizes. Results highlight the importance of the mucus layer in hindering the migration of particles > 200 nm and identify compositions diffuse more easily through mucus.

Summary of Research:

Over 400 million tons of plastic are produced every year [1]. Many of these plastics end up in the environment, gradually breaking down into microplastics. Microplastics are defined as plastic particles under 5 mm and can be found in the water soil and air. Ingestion of these particles has been linked to negative health impacts including metabolic disorders, neurotoxicity and intestinal inflammation [2]. The mucus layer within the intestine acts as a protective barrier against harmful substances however, studies have demonstrated that microplastics often travel through intestinal mucus and end up in other organs [3]. The goal of this research project is to characterize microplastic migration through intestinal mucus to identify key factors contributing to microplastic migration and understand the role of the mucus layer. Previous work has looked at particle migration in various mucus models such as porcine gastric mucus [4], hydrogels, human lungs, human cervix and various animal sources [4,5]. Most studies focus on polystyrene microplastics however a broad array of particle compositions are often ingested [2]. We used particle characterization techniques and microrheology to study the migration of different compositions, surface functionalizations and sizes in intestinal mucus produced by HT29MTX human colorectal adenocarcinoma cells.

HT-29MTX cells were chosen due to their high mucus production and common use in human intestinal studies. Cells were grown as a monolayer in growth media for 21 days for a mature mucus layer. Zeta potential was used to measure the effective surface charge of particles in solution. Zeta potential was measured using a Malvern Nano Zs Zetasizer (Malvern Pananalytical, Malvern, U.K.). A total of three measurements were taken for each particle type. Each particle composition and functionalization was tested with values ranging from -43 mV to 14 mV, as shown in Figure 1.

Cells were cultured in 6-well plates on circular cover glasses for microrheology to determine particle diffusivity. The particle of interest was added to the culture media at a concentration of 1 μl/ml and left to equilibrate for 15 minutes. The diffusion of particles through the mucus layer was imaged on an Elyra Super Resolution Microscope. A time series was collected with a step of 0.05 s with at least three biological replicates and at different locations over the cell monolayer. Images were analyzed using ImageJ Trackmate and Matlab to determine mean squared displacements and diffusion coefficients [6].

Diffusivity was determined to compare the effects of size, composition and surface functionalization. Diffusivity increased as microplastic size decreased, as shown in Figure 2. Polyethylene and polystyrene particles had the highest diffusivity out of all particle compositions tested, while silica particles had the lowest diffusivity. The diffusivity of 500 nm particles could not be determined

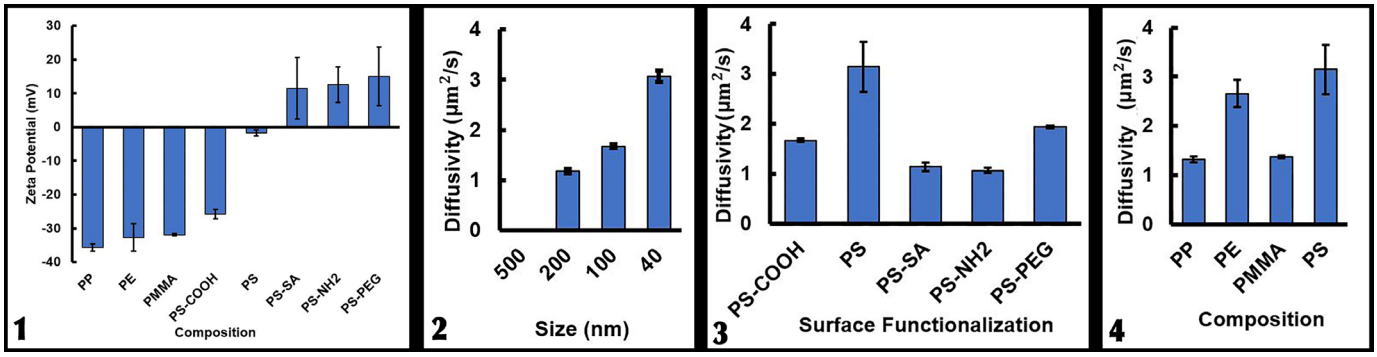

Figure 1: Zeta potential for each particle composition and surface functionalization.

Figure 2: Diffusivity for each particle size.

Figure 3: Diffusivity for each particle composition at 100 nm for PS, PP, PE, and PMMA.

Figure 4: Diffusivity for each surface functionalization of for PS 100 nm particles.

as these particles did not migrate through the mucus. Mucus has a pore size of approximately 200 nm, which prevented these particles from passing through [7]. In contrast, 40 nm particles were able to diffuse much more easily through the mucus layer. Figures 3 and 4 indicate that unfunctionalized polystyrene had the highest diffusivity. These results highlight the role of the mucus layer in preventing the migration of particles > 200 nm and indicate that certain compositions present a greater health threat. Further study is needed to understand how diffusivity might be related to negative health effects such as inflammation and cell death.

Conclusions and Future Steps:

The tools and technical expertise provided at the CNF was essential to the rapid testing necessary for biological samples. Future work will investigate how the mucus layer structure and mechanical properties alter cell uptake of particles through the design of microfluidic chips for cell growth and imaging. We will also expand on our preliminary tests to include particles carrying other environmental pollutants which may alter surface properties and change particles migration through the mucus.

References:

[1] Y. Li, L. Tao, Q. Wang, F. Wang, G. Li, M. Song, Environ. Health 2023, 1, 249.

[2] G. Visalli, A. Facciolà, M. Pruiti Ciarello, G. De Marco, M. Maisano, A. Di Pietro, Int J Environ Res Public Health 2021, 18, 5833.

[3] M. M. Garcia, A. S. Romero, S. D. Merkley, J. L. Meyer-Hagen, C. Forbes, E. E. Hayek, D. P. Sciezka, R. Templeton, J. Gonzalez-Estrella, Y. Jin, H. Gu, A. Benavidez, R. P. Hunter, S. Lucas, G. Herbert, K. J. Kim, J. Y. Cui, R. R. Gullapalli, J. G. In, M. J. Campen, E. F. Castillo, Environmental Health Perspectives 2024, 132, 047005.

[4] P. Georgiades, P. D. A. Pudney, D. J. Thornton, T. A. Waigh, Biopolymers 2014, 101, 366.

[5] A. Cobarrubia, J. Tall, A. Crispin-Smith, A. Luque, Frontiers in Physics 2021, 9.

[6] J.-Y. Tinevez, N. Perry, J. Schindelin, G. M. Hoopes, G. D. Reynolds, E. Laplantine, S. Y. Bednarek, S. L. Shorte, K. W. Eliceiri, Methods 2017, 115, 80.

[7] J. McCright, A. Sinha, K. Maisel, Cell Mol Bioeng 2022, 15, 479.

Fabrication of Non-Volatile Memory Transistors Using Hybrid Two-Dimensional Materials

CNF Project Number: 3064-23
Principal Investigator(s): Yu Zhong
User(s): Haolei Zhou, Qiyi Fang, Kaushik Chivukula, Ashutosh Garudapalli

Affiliation(s): Department of Materials Science and Engineering, Cornell University

Primary Source(s) of Research Funding: Cornell Startup Funding

Contact: yz2833@cornell.edu, hz595@cornell.edu, qf52@cornell.edu, kc836@cornell.edu, ag2289@cornell.edu

Research Group Website: https://zhong.mse.cornell.edu/

Primary CNF Tools Used: Oxford 100 PECVD, DWL 2000 Mask Writer, DWL 66FS Writer, Odd Hour Evaporator, Even Hour Evaporator, ABM Contact Aligner

MATERIALS

Abstract:

This project is focused on the fabrication of electrolyte-gated nonvolatile memory transistors based on hybrid two-dimensional (2D) materials. The goal is to understand how the hysteresis changes under various measurement conditions for a memory transistor made from a hybrid MoS_2-crow ether thin film. The retainability of ions inside the film is the main factor of such a hysteresis phenomenon. Previous research shows that the MoS_2-based transistors may have a small hysteresis at high gate voltage or due to factors such as high moisture absorption [1]. In our experiment, we used liquid electrolytes instead of typical solid-state electrolytes. By applying this change, we found a much lower turn-on voltage and a much larger hysteresis. In addition, by adding a thin layer of a 2D crown ether polymer (CEP) film on top of monolayer MoS_2, the retention time of ions seems to increase and hence increases the hysteresis. Such hysteresis is critical for neuromorphic computing such as potentiation or depression.

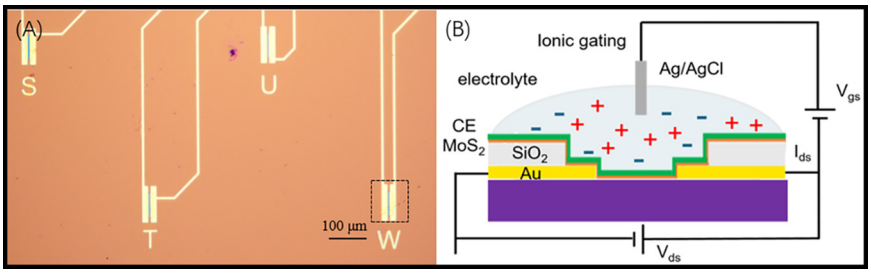

Figure 1: (A) Optical image of fabricated FET device covered with MoS_2 single layer film and (B) Schematic of the memory transistor.

Summary of the Research:

To synthesize CEP films, we used a method called laminar assembly polymerization in a homemade Teflon reactor [2]. The CEP films were grown at the interface between water and pentane. In the bottom of the reactor, 2,4,6-trihydroxybenzene-1,3,5-tricarbaldehyde was dissolved in deionized water. For the injected solution, 6,7,9,10,17,18,20,21-octahydrodibenzo[b,k][1,4,7,10,13,16]hexaoxacyclooctadecine-2,13-diamine dissolved in a solution of mixed chloroform and methanol with a ratio of 3:1 was delivered through the top pentane phase. By gradually injecting the solution, the CEP film was formed at the interface.

For the device fabrication, a set of lithographic tools at Cornell NanoScale Facility was used. Figure 1 shows an optical image and schematic of the device. To make the device, a contact alignment mask was first made. The patterns of masks were tested via DWL 66FS writer. There are two masks made by DWL 2000 mask writer. The first mask is for defining the metal contacts. the basic structure of the device with a channel length of 150 micrometers and a channel width of 10 micrometers.

A 280 nm silicon dioxide is deposited on the p-doped pure silicon by the plasma-enhanced chemical vapor deposition. Then S1813 was spin-coated on the substrate with a recipe of 5000 rpm – 40s. ABM contact aligner is then used for exposing the photoresist. MIF-726 60s recipe was applied to develop the photoresist. The deposition of a 10 nm Ti/ 100 nm Au electrode was accomplished by the odd-hour evaporator with a ratio of

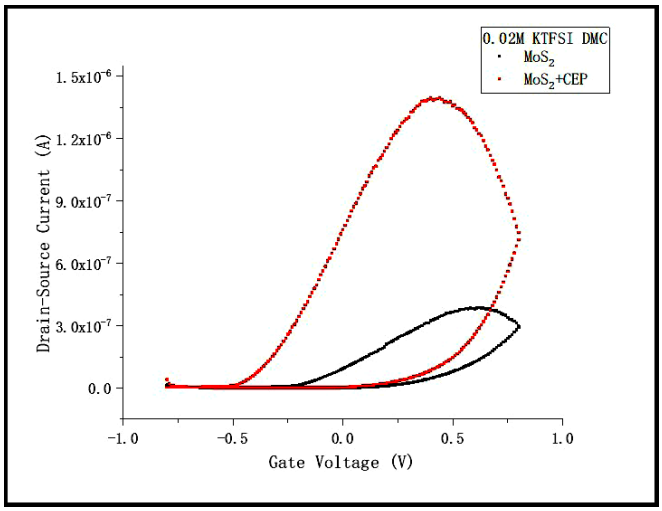

Figure 2: Transfer curve of MoS2 devices with (red) and without CEP film (black).

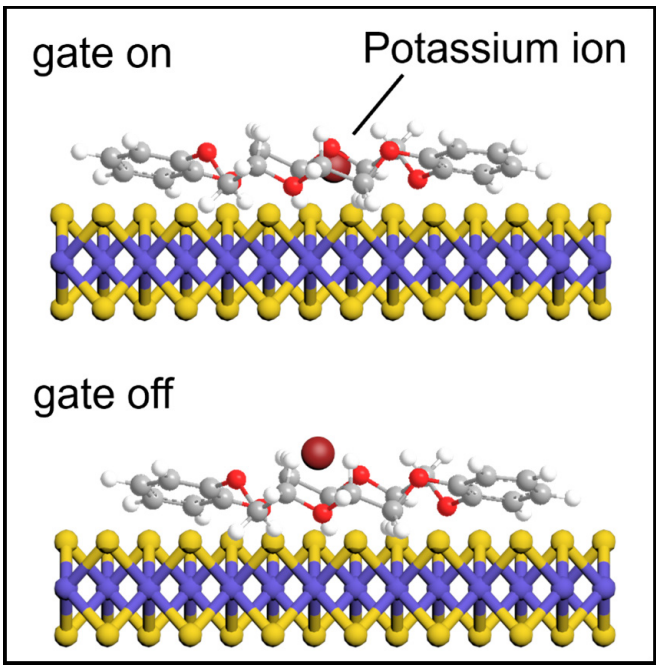

Figure 3: Schematic of memory effect from a MoS2-CEP film.

one angstrom per second at a power of approximately 10%. The liftoff process was done with 20 minutes of S1165 remover, 20 minutes of acetone and five minutes of isopropanol. The second mask is designed for the insulating layer. The same processes were done except for the deposition part. 80nm of silicon oxide was deposited on the device with the even-hour evaporator. The rate was approximately 3.5 angstrom per second at a power of 3%.

To complete the device fabrication, we first transferred MoS2 on the prepatterned electrode mentioned above followed by transferring the CEP film on MoS2. We compared the transfer curve of MoS2 transistors with and without CEP film. The device with a CEP film shows a more significant hysteresis than that without a CEP film (Figure 2). Our hypothesis is that the presence of CEP film can increase the retention time of ions on the MoS2 surface due to the strong interaction between the cations and crown ether units (Figure 3). Further investigations are underway to reveal the mechanisms for the memory effect.

Conclusions and Future Plans:

The MoS2 device exists some hysteresis intrinsically in the liquid electrolyte. Such hysteresis is closely correlated with the concentration of the liquid electrolyte and the dielectric constant of the solvent. The addition of CEP film will increase the retainability of ions on the films because of strong cation-crown ether interactions. In the future, a device with better performance (lower channel width) can be designed to reduce the effect of the leakage current.

References:

[1] Late, D. J.; Liu, B.; Matte, H. S. S. R.; Dravid, V. P.; Rao, C. N. R., Acs Nano 2012, 6 (6), 5635-5641.

[2] Zhong, Y.; Cheng, B.; Park, C.; Ray, A.; Brown, S.; Mujid, F.; Lee, J.-U.; Zhou, H.; Suh, J.; Lee, K.-H.; Mannix, A. J.; Kang, K.; Sibener, S. J.; Muller, D. A.; Park, J. Science 2019, 366 (6471), 1379-1384.

FuSe Internship

CNF Project Number: CNF Summer Internship
Principal Investigator(s): Ron Olson[1], Lynn Rathbun[1]
User(s): Sherri Ellis[2]

Affiliation(s): 1. Cornell NanoScale Science & Technology Facility (CNF), Cornell University; 2. Engineering Program, Tompkins Cortland Community College

Primary Source(s) of Research Funding: Cornell NanoScale Science & Technology Facility (CNF), a member of the National Nanotechnology Coordinated Infrastructure NNCI), which is supported by the National Science Foundation (Grant NNCI-2025233)

Contact: olson@cnf.cornell.edu, rathbun@cnf.cornell.edu, see43@cornell.edu

Research Group Website: https://www.cnf.cornell.edu/

Primary CNF Tools Used: Hamatech Hot Piranha & Wafer Processers, YES EcoClean Asher, SÜSS Microtec Gamma Cluster System, Heidelberg DWL 2000 Mask Writer, ABM Contact Mask Aligner, ASML PAS 5500/300C DUV Wafer Stepper, Oxford 1000 Plasma Enhanced Chemical Vapor Deposition (PECVD) System, FilMetrics F50, Zeiss Scanning Electron Microscopes (SEMs), Veeco Icon Atomic Force Microscope (AFM).

Abstract:

I am participating in the Future of Semiconductors (FuSe) internship, a new collaboration between the Cornell Nanoscale Facility (CNF), Tompkins Cortland Community College (TC3), the University of Chicago and the University of Wisconsin-Madison. This internship includes learning about micro and nano fabrication, using CNF's cleanroom tools and processes, assisting with tasks in the photolithography areas, and providing support to a research project focused on new resist polymers. I have completed seven weeks of the 16-week internship.

Summary of Research:

I began with learning about cleanroom tools through CULearn's online courses and participating in CNF's short course "Technology & Characterization at the Nanoscale." This was followed by hands-on training and practice with some of CNF's cleanroom tools and assisting with daily and weekly tasks in the photolithography areas.

The processes and tools that I have been trained in and utilized include the following: For cleaning wafers, I used the hot strip bath, spin rinse dryers, Hamatech Hot Piranha, YES EcoClean Asher, and Glen 1000. For applying wafer coating by hand, I used spinners, hotplates, and the FilMetrics F50 to measure the photoresist film thickness. For automated wafer coating and post exposure developing, I ran the SUSS Microtec Gamma Cluster System.

For making masks, I learned how to use KLayout / L-edit CAD software to create the design, and the Heidelberg DWL 2000 Mask Writer to create the masks. To expose the coated wafers with a mask, I operated the ABM Contact Mask Aligner (figure 1) and the ASML PAS 5500/300C DUV Wafer Stepper. For developing the photoresist after exposure, I used the Hamatech Wafer Processors. I was also trained on the Oxford 1000 Plasma Enhanced Chemical Vapor Deposition (PECVD) system for thin film deposition.

For microscopy, I have operated basic optical microscopes, Zeiss Scanning Electron Microscopes (SEMs) (figure 2), and the Veeco Icon Atomic Force Microscope (AFM). I may also still receive training on the JEOL 6300 Electron Beam Lithography System.

I was offered the opportunity to prepare wafers for use in training, using a specific recipe through a multistep process. Some of the wafers were previously used, so I first cleaned them by spinning with acetone/IPA, using the hot strip bath, the spin rinse dryer, the Ecoclean, and the Hot Piranha. Once prepared, I coated the wafers on a spinner, baked them, assessed thickness with FilMetrics F50, exposed them using the ABM Contact Aligner, developed them in a Hamatech, and completed the process with a hard bake. I appreciated being able to engage in a multistep photolithography process in service of a useful finished product.

Regarding assisting with daily and weekly tasks in the photolithography rooms, this included cleaning, refilling and restocking chemicals and supplies, refilling

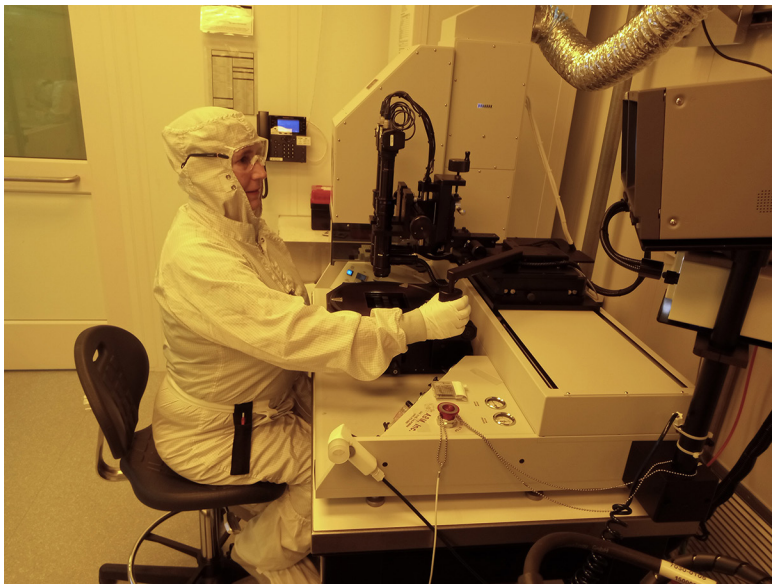

Figure 1: Ellis at the ABM Contact Mask Aligner.

Figure 2: Ellis at the Zeiss Scanning Electron Microscope (SEM).

chemicals in the Hamatechs and Hot Piranha, and refilling water in the Gamma, ASML, and DWL 2000.

For the second half of my internship, I will continue to help with tasks in the photolithography areas and assist a Ph.D. student with research focused on developing a new resist polymer. Per the student, the project "focuses on using a block copolymer with an ideally high χ (chi) value to improve etching contrast, applying directed self-assembly as a strategy to increase pattern density."

This internship has been a valuable learning experience so far. I am so grateful for this opportunity to learn about photolithography processes and tools, and to have so many hands-on experiences in the cleanroom. I'm looking forward to further training, continuing to assist in the photolithography areas, and participating in the innovative research project.

Acknowledgements:

Special thanks to the following CNF staff for their supervision, training, and support: Ron Olson, Garry Bordonaro, Giovanni Sartorello, John Treichler, Xinwei Wu, Aaron Windsor, Jeremy Clark, and Alan Bleier, and to Ph.D. student Chaoqiuyu (Rachel) Wang for the opportunity to assist in her research.